DOE Project

Nonequilibrium Physics and Phase-Field Modeling of Multiphase Flow in Porous Media

Grant Number DE-SC0003907

Final Report

Original Period of Performance: March 1, 2010 – February 28, 2015
No-cost Extension: March 1, 2015 – February 28, 2016

Principal Investigator: Ruben Juanes
Massachusetts Institute of Technology

September 1, 2016

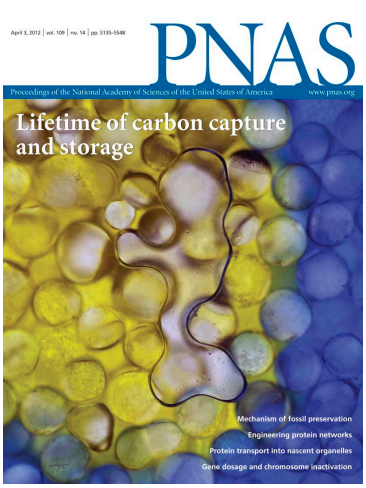

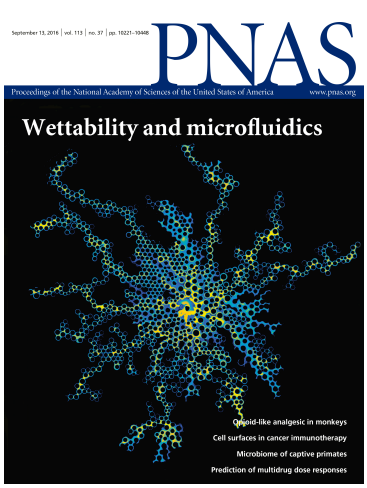

Contents

1 Project objectives

Carbon capture and geologic storage, dissociation of methane hydrates in permafrost, enhanced oil recovery, and water dropout in low-temperature fuel cells, all have something in common: two or more fluids flow simultaneously through a porous medium; and the displacement of one fluid by another is often unstable (either due to gravity or viscous forces). Yet, our ability to model multiphase flow mathematically at the macroscale has remained a challenge. The traditional equations are unable to predict, explain, or even reproduce, the formation of the complex patterns observed in experiments.

The overarching goal of this proposal is to develop a new continuum theory of multiphase flow in porous media following a phase-field modeling approach, which recognizes that the system is out of thermodynamic equilibrium. The specific objectives are organized in three main thrusts:

1. Immiscible fluid displacements in a capillary tube and a Hele-Shaw cell.
2. Multiphase flow in porous media.
3. Application to CO_2 storage in saline aquifers.

We propose a radical new approach—phase-field modeling—to advance our fundamental understanding and predictive capabilities of multiphase porous media flow. The basic tenet, with origins in the mathematical description of solidification processes, is that the system is far from equilibrium, and the energy of the system is a function of the inhomogeneous distribution of fluid phases in the pore space. This leads naturally to higher-order terms in the mass conservation equations. In recent work, we have used this formalism to develop a theory that explains and quantitatively predicts the formation of gravity fingers during infiltration into dry soil. The success of this application suggests that continuum models derived using the phase-field modeling framework have the potential to predict unstable multiphase flow in porous media.

The research agenda is organized around *a set of hypothesis* on hitherto unexplained behavior of multiphase flow. All these hypothesis are nontrivial, and *testable*. Indeed, a central aspect of the proposal is that we will test each of them by means of carefully-designed laboratory experiments, therefore probing the validity of the proposed theory.

Finding a parsimonious macroscopic theory of multiphase flow through porous media is an open scientific problem. If successful, this proposal will provide a continuum mathematical framework that predicts the stability–instability of fluid displacement at large scales. This would be a landmark result in soft-matter physics, leading to fundamental advances in the deployment of energy systems (oil and gas recovery, CO_2 sequestration, fuel cells, microfluidics), which depend crucially on the formation and control of fluid-fluid instabilities.

2 Introduction and organization of the report

The overarching goal of this project was to develop a new continuum theory of multiphase flow in porous media. The theory follows a phase-field modeling approach, and therefore has a sound thermodynamical basis. It is a phenomenological theory in the sense that its formulation is driven by macroscopic phenomena, such as viscous instabilities during multifluid displacement. The research agenda was organized around *a set of hypothesis* on hitherto unexplained behavior of multiphase flow. All these hypothesis are nontrivial, and *testable*. Indeed, a central aspect of the project was testing each hypothesis by means of carefully-designed laboratory experiments, therefore probing the validity of the proposed theory.

The proposed research places an emphasis on the fundamentals of flow physics, but is motivated by important energy-driven applications in earth sciences, as well as microfluidic technology. The report is organized following the three main thrusts of the original proposal, in which we address the following scientific questions:

1. *Fluid-fluid displacements in a Hele-Shaw cell.* (1) How can wetting be incorporated into the phase-field model, and how does it affect the instability? (2) How does the transition to unstable behavior depend on surface tension? (3) Are nonequilibrium effects (capillary number-dependent contact angle) stabilizing or de-stabilizing?
2. *Multiphase flow in porous media.* (1) Can we develop a phase-field model that provides a continuum version of Lenormand's diagram? (2) How do the velocity and width of viscous fingers scale with viscosity contrast, capillary number, and wetting properties? (3) How is viscous fingering affected by the medium heterogeneity?
3. *Application to CO_2 storage in saline aquifers.* (1) What displacement patterns should we expect for typical conditions of geological CO_2? (2) How does the amount of capillary trapping depend on displacement efficiency? (3) How do fluid instabilities and capillary pressure hysteresis affect storage efficiency?

3 MIT personnel supported

- Luis Cueto-Felgueroso (postdoctoral associate), 2010–2013
- Jane Chui (PhD student), 2014–2016
- Xiaojing Fu (PhD student), 2012–2014
- Christos Nicolaides (PhD student), 2012–2014
- Amir Pahlavan (PhD student), 2012–2016
- Michael Szulczewski (PhD student), 2010–2013
- Benzhong Zhao (PhD student), 2013–2016

4 Fluid-fluid displacements in a Hele-Shaw cell

Flow in a Hele-Shaw cell—two parallel plates separated by a thin gap—has played a central role in the development of hydrodynamics theory and the study of fluid instabilities. It also has direct practical applications, since current microfluidic fabrication techniques often lead to planar flow configurations. A sketch of immiscible fluid displacement in a Hele-Shaw cell is shown in Figure 1. The displacement front will, in general, show an interface that is curved both on the plane of the cell—due to instability—and on the vertical cross section—due to wetting effects.

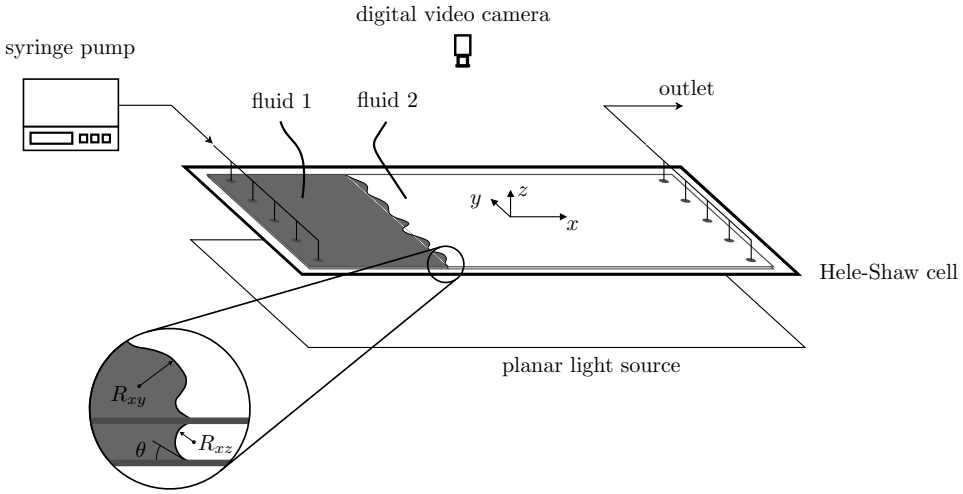

Figure 1. Sketch of an immiscible linear displacement in a Hele-Shaw cell. Fluid 1 (gray) displaces fluid 2 (white). The displacement front will, in general, show an interface that is curved both on the plane of the cell—due to instability—and on the vertical cross section—due to wetting effects (see inset).

4.1 Modeling wetting

4.1.1 Macroscopic phase-field model of partial wetting: bubbles in a capillary tube [3]

Drops and bubbles are non-spreading, local, compactly supported features. They are also equilibrium configurations in partial wetting phenomena. Yet, current macroscopic theories of capillary-dominated flow are unable to describe these systems. We propose a framework to model multiphase flow in porous media with non-spreading equilibrium configurations. We illustrate our approach with a one-dimensional model of two-phase flow in a capillary tube. Our model allows for the presence of *compactons*: non-spreading steady-state solutions in the absence of external forces (Fig. 2). We show that local rate-dependency is not needed to explain globally rate-dependent displacement patterns, and we interpret dynamic wetting transitions as the route from equilibrium, capillary-dominated configurations, towards viscous-dominated flow. Mathematically, these transitions are possible due to non-classical shock solutions and the role of bistability and higher-order terms in our model.

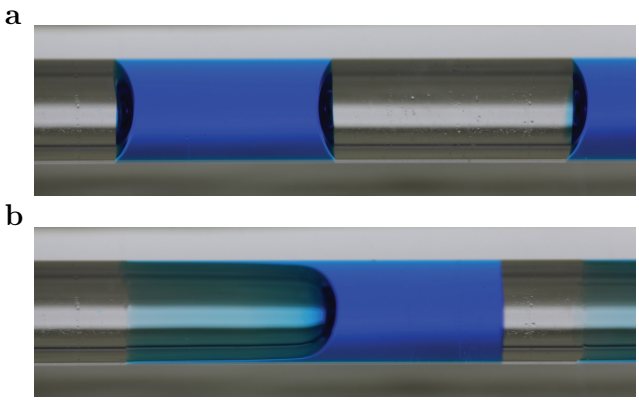

Figure 2. Statics and dynamics of fluid slugs in a capillary tube. **a**, Static configuration of an air bubble (transparent) between two slugs of water (dyed blue) in a glass capillary tube. The liquid-gas interface exhibits a well-defined contact angle, characteristic of a system with partial wetting. **b**, Snapshot of an advancing liquid slug, blown by air from left to right. The leading interface advances with a contact angle that is larger than the static contact angle. At the back end of the slug, air penetrates through the center of the tube and leaves a macroscopic film of viscous fluid attached to the walls. The advancing contact angle and the film thickness are rate-dependent.

4.1.2 A phase-field model of two-phase Hele-Shaw flow [4]

We propose a continuum model of two-phase flow in a Hele-Shaw cell. The model describes the multiphase, three-dimensional flow in the cell gap using gap-averaged quantities such as fluid saturations and Darcy fluxes. Viscous and capillary coupling between the fluids in the gap leads to a nonlinear fractional flow function. Capillarity and wetting phenomena are modeled within a phase-field framework, designing a heuristic free energy functional that induces phase segregation at equilibrium. We test the model through the simulation of bubbles and viscously-unstable displacements (viscous fingering; Fig. 3). We analyze the model's rich behavior as a function of capillary number, viscosity contrast and cell geometry. Including the effect of wetting films on the two-phase flow dynamics opens the door to exploring, with a simple, two-dimensional model, the impact of wetting and flow rate on the performance of microfluidic devices and geologic flows through fractures.

4.1.3 Two fluid flow in a capillary tube [18]

The displacement of a fluid such as water by an injected finger of air in a narrow tube is a classic problem of fluid mechanics. Since the early experimental and theoretical work of Bretherton and Taylor, there has been much research on the injection of one fluid into a different fluid resident in a thin tube. Characterizing such flows is significant not only for small scale fluid devices but also for modeling macroscopic two fluid flow in porous media. In this paper, we consider a recent model that incorporates ideas from phase field theory, resulting in a fourth order nonlinear partial differential equation (PDE) similar to the PDE of thin liquid films. The PDE possesses a spinodal-type instability at long wavelengths that we associate with the physical varicose or Plateau instability, in which the cylindrical gas finger, of sufficient length and for a range of widths, tends to break up into bubbles.

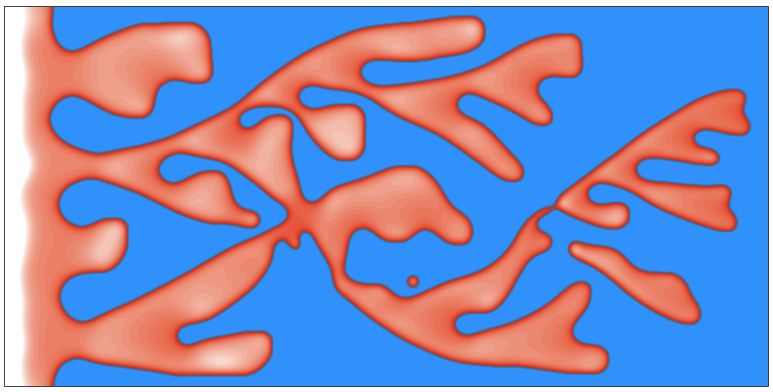

Figure 3. Pinchoff and reconnection in unstable displacements at large Ca and M. Here we show a snapshot of the simulation for M=500 and Ca=0.01 at late times. The interaction between fingers results in pinch off and reconnection of fingers, and isolated bubbles that arise due to Rayleigh-Plateau instabilities (see Supplementary Movie 1).

4.1.4 Thin films in partial wetting: internal selection of contact-line dynamics [1]

When a liquid touches a solid surface, it spreads to minimize the system's energy. The classic thin-film model describes the spreading as an interplay between gravity, capillarity and viscous forces, but cannot see an end to this process as it does not account for the nonhydrodynamic liquid–solid interactions. While these interactions are important only close to the contact line, where the liquid, solid and gas meet, they have macroscopic implications: in the partial-wetting regime, a liquid puddle ultimately stops spreading. We show that by incorporating these intermolecular interactions, the free energy of the system at equilibrium can be cast in a Cahn–Hilliard framework with a height-dependent interfacial tension. Using this free energy (Fig. 4), we derive a mesoscopic thin-film model that describes statics and dynamics of liquid spreading in the partial-wetting regime. The height-dependence of the interfacial tension introduces a localized apparent slip in the contact-line region and leads to compactly-supported spreading states. In our model, the contact line dynamics emerge naturally as part of the solution and are therefore nonlocally coupled to the bulk flow. Surprisingly, we find that even in the gravity-dominated regime, the dynamic contact angle follows the Cox–Voinov law.

4.1.5 Wettability control on multiphase flow in patterned microfluidics [26]

Multiphase flow in porous media is important in many natural and industrial processes, including geologic CO_2 sequestration, enhanced oil recovery, and water infiltration into soil. Although it is well known that the wetting properties of porous media can vary drastically depending on the type of media and pore fluids, the effect of wettability on multiphase flow continues to challenge our microscopic and macroscopic descriptions. Here, we study the impact of wettability on viscously unfavorable fluid-fluid displacement in disordered media by means of high-resolution imaging in microfluidic flow cells patterned with vertical posts (Fig. 5). By systematically varying the wettability of the flow cell over a wide range of contact angles, we find that increasing the substrate's affinity to the injected fluid results in more efficient displacement of the defending fluid up to a critical wetting transition, beyond which the trend is reversed. We identify the pore-scale

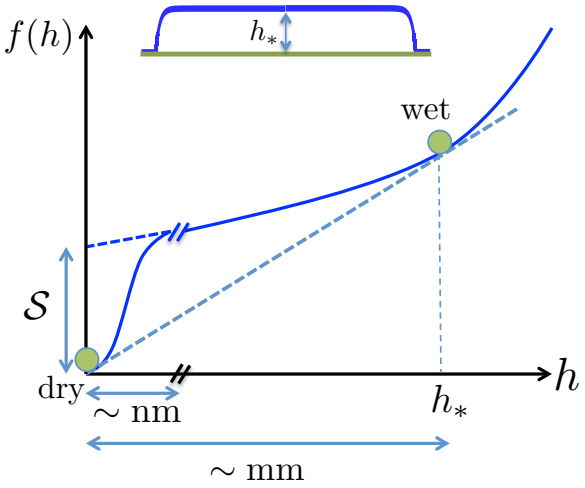

Figure 4. Schematic of the tangent construction on the bulk free energy, $f(h)$, leading to the coexistence of wet, $h = h_*$, and dry, $h = 0$, states. In the absence of intermolecular forces, the bulk free energy does not reduce to the solid–gas interfacial energy as $h \to 0$ unless $\mathcal{S} = 0$, which implies complete wetting.

mechanisms—cooperative pore filling (increasing displacement efficiency) and corner flow (decreasing displacement efficiency)—responsible for this macroscale behavior, and show that they rely on the inherent 3D nature of interfacial flows, even in quasi-2D media. Our results demonstrate the powerful control of wettability on multiphase flow in porous media, and show that the markedly different invasion protocols that emerge—from pore-filling to post-bridging—are determined by physical mechanisms that are missing from current pore-scale and continuum-scale descriptions.

4.2 Transition to miscibility

4.2.1 Fluid mixing from viscous fingering [13, 14]

Mixing efficiency at low Reynolds numbers can be enhanced by exploiting hydrodynamic instabilities that induce heterogeneity and disorder in the flow. The unstable displacement of fluids with different viscosities, or viscous fingering, provides a powerful mechanism to increase fluid-fluid interfacial area and enhance mixing (Fig. 6). Here we describe the dissipative structure of miscible viscous fingering, and propose a two-equation model for the scalar variance and its dissipation rate. Our analysis predicts the optimum range of viscosity contrasts that, for a given Péclet number, maximizes interfacial area and minimizes mixing time. In the spirit of turbulence modeling, the proposed two-equation model permits upscaling dissipation due to fingering at unresolved scales.

4.2.2 Synergetic fluid mixing from viscous fingering and alternating injection [15]

We study mixing of two fluids of different viscosity in a microfluidic channel or porous medium. We show that the synergetic action of alternating injection and viscous fingering leads to a dramatic increase in mixing efficiency at high Péclet numbers. Based on observations from high-resolution simulations, we develop a theoretical model of mixing efficiency that combines a hyperbolic mixing model of the channelized region ahead, and a mixing–dissipation model of the pseudo-steady

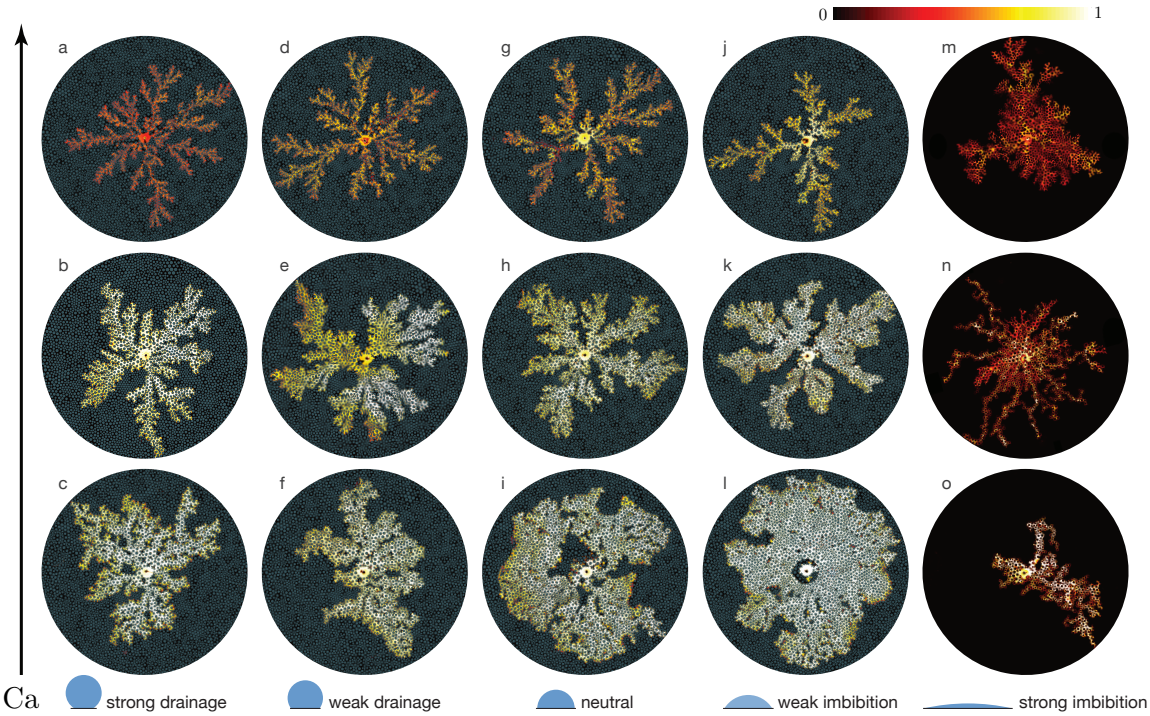

Figure 5. Displacement patterns for different wettability conditions in a micromodel patterned with cylindrical posts (left to right: $\theta = 150^\circ,\ 120^\circ,\ 90^\circ,\ 60^\circ,\ 7^\circ$) and capillary numbers (bottom to top: $\mathrm{Ca} = 2.9 \times 10^{-3}, 2.9 \times 10^{-2}, 2.9 \times 10^{-1}$). These patterns correspond to the end of the experiment, which is when the invading fluid reaches the perimeter of the flow cell. The colormap shows the gap-averaged saturation of the invading water. The pattern of circular posts is overlaid on the experimental images and all images are oriented in the same way to aid visual comparison. Generally, the displacement becomes more efficient as the flow cell becomes more hydrophilic (*i.e.*, decreasing θ), or as Ca decreases. These trends do not hold for strong imbibition (m–o), which has a very low displacement efficiency for all Ca.

region behind. Our macroscopic model quantitatively reproduces the evolution of the average degree of mixing along the flow direction, and can be used as a design tool to optimize mixing from viscous fingering in a microfluidic channel.

4.2.3 Interface evolution during radial miscible viscous fingering [2]

We study experimentally the miscible radial displacement of a more viscous fluid by a less viscous one in a horizontal Hele-Shaw cell (Fig. 8). For the range of tested injection rates and viscosity ratios we observe two regimes for the evolution of the fluid-fluid interface. At early times the interface length increases linearly with time, which is typical of the Saffman-Taylor instability for this radial configuration. However, as time increases, interface growth slows down and scales as $\sim t^{\frac{1}{2}}$, like one expects in a stable displacement, indicating that the overall flow instability has shut down. Surprisingly, the crossover time between these two regimes decreases with increasing injection rate. In this letter we propose a theoretical model that is consistent with our experimental results, explains the origin of this second regime, and predicts the scaling of the crossover time with injection rate and the mobility ratio. The key determinant of the observed scalings is the competition between advection and diffusion time scales at the displacement front, suggesting that

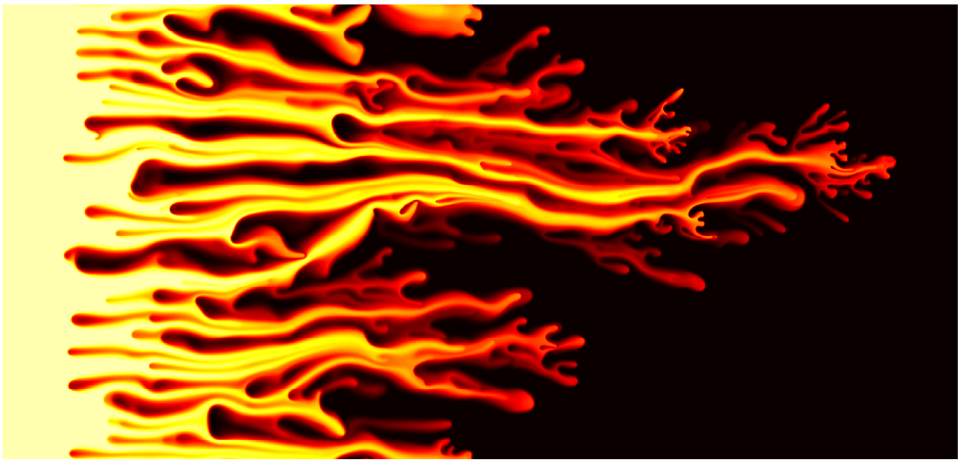

Figure 6. Snapshot of the concentration field during the unstable displacement of a more viscous fluid (dark) by a fully-miscible, less viscous fluid (light). The formation, splitting, and nonlinear interaction of viscous fingers induce disorder in the velocity field that affects the mixing rate between the fluids. The displacement corresponds to a viscosity ratio $M = \exp(3.5) \approx 33$ and Péclet number $\mathrm{Pe} = 10^4$.

our analysis can be applied to other interfacial-evolution problems such as the Rayleigh–Bénard–Darcy instability.

4.2.4 Thermodynamic coarsening arrested by viscous fingering in partially-miscible binary mixtures [8]

We study the evolution of binary mixtures far from equilibrium, and show that the interplay between phase separation and hydrodynamic instability can arrest the Ostwald ripening process characteristic of non-flowing mixtures. We describe a model binary system in a Hele-Shaw cell using a phase-field approach with explicit dependence of both phase fraction and mass concentration. When the viscosity contrast between phases is large (as is the case for gas and liquid phases), an imposed background flow leads to viscous fingering, phase branching and pinch-off (Fig. 9). This dynamic flow disorder limits phase growth and arrests thermodynamic coarsening. As a result, the system reaches a regime of statistical steady state in which the binary mixture is permanently driven away from equilibrium.

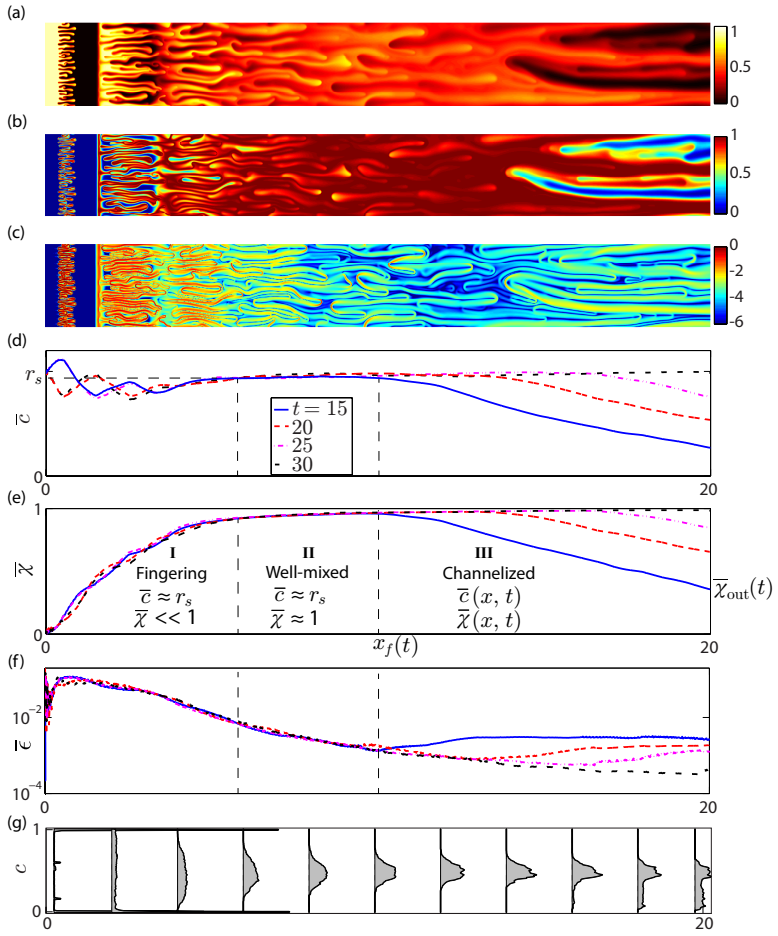

Figure 7. Snapshot of the concentration field during the alternating injection of more viscous (dark) and less viscous (light) fluids. Viscous fingering at the displacement front promotes mixing of the two fluids. At high viscosity contrast, however, a few dominating fingers coalesce to form persistent channels. These channels serve as preferential pathways for subsequent slugs of the less viscous fluid, inhibit transverse mixing, and shield growth of adjacent fingers. (a) Concentration c, (b) degree of mixing χ, and (c) scalar dissipation rate $\log \epsilon$ from an alternating injection simulation with viscosity ratio $M{=}\exp(2){\approx}7$ and Péclet number Pe$=$2000 at time $t{=}18.6$. The degree of mixing is high (red) where mixing has already taken place. Scalar dissipation rate is high (red) at the interfaces where the fluid is actively being mixed. (d), (e), and (f) are longitudinal profiles of concentration $\overline{c}$, degree of mixing $\overline{\chi}$, and scalar dissipation rate $\overline{\epsilon}$, averaged over a moving time-window (of duration equal to 3 injection cycles, although the same behavior holds for different averaging windows). $\overline{\epsilon}$ reaches a maximum where fingering begins and a minimum where channeling begins, congruent with a non-monotonic degree of mixing $\overline{\chi}$ with x. (g) The time-averaged PDF of concentration evolves from two delta-like functions (segregated pure fluids near $x{=}0$ in Region I) to a Gaussian-like function (well-mixed fluids in Region II) to an anomalous distribution (channeling in Region III). The vertical dashed lines indicate the boundaries of the three mixing regions at time $t{=}15$; x_f denotes the position of the well-mixed front, which is the position of the maximum longitudinal degree of mixing in the domain, $\overline{\chi}_f$, at a given time.

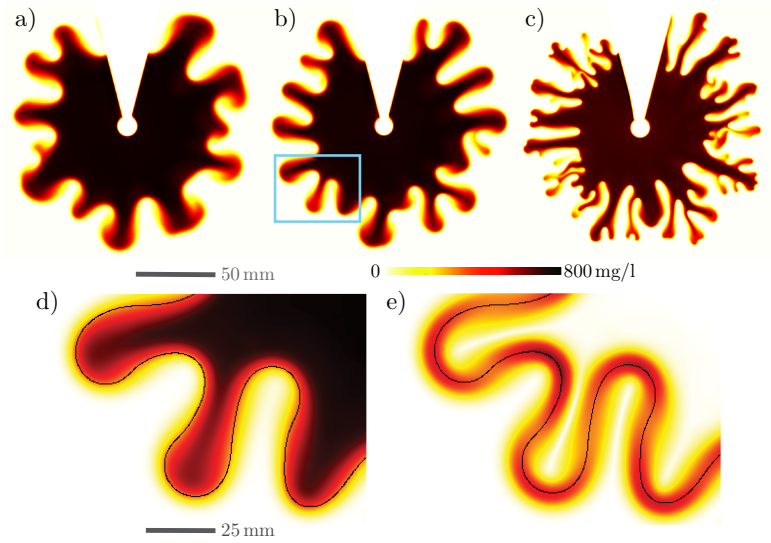

Figure 8. a), b), and c) are concentration fields of the injected fluid displacing a more viscous one (viscosity contrast $M = 10$) at the center of a Hele-Shaw cell at three different flow rates ($Q = 0.004$, 0.008, and 0.02 mL/min, at $t = 5508$, 2416 and 1214 seconds after the start of injection, respectively). d) and e) are magnifications of the concentration field and its gradient, respectively. The black line represents the location of the fluid-fluid interface, defined as the locus of the local maxima of the concentration gradient.

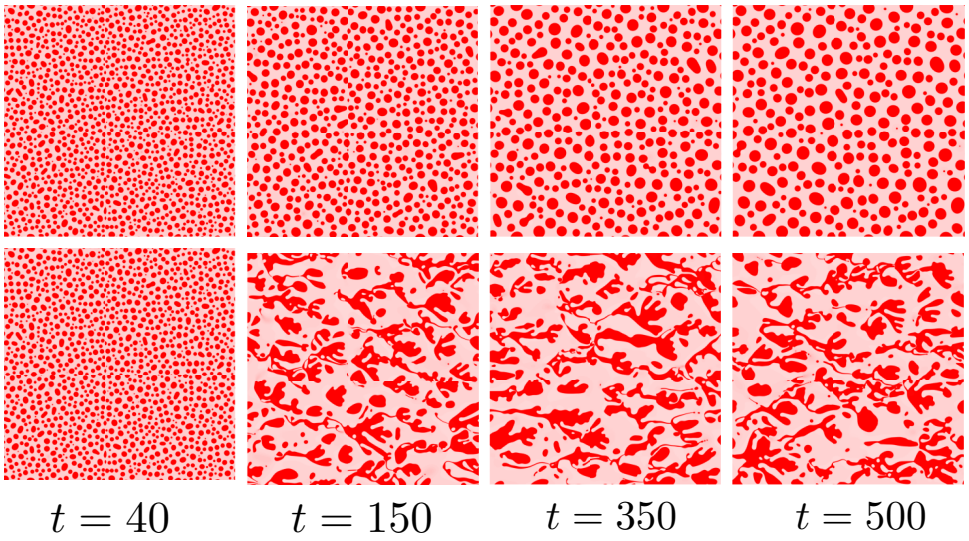

Figure 9. Snapshots of concentration in a binary mixture at t=40, 150, 350 and 500, under no flow (top) and with periodic left-to-right flow imposed at t>40 (bottom).

5 Multiphase flow in porous media

5.1 Unstable displacements

5.1.1 Capillary fracturing in granular media [12]

We study the displacement of immiscible fluids in deformable, non-cohesive granular media. Experimentally, we inject air into a thin bed of water-saturated glass beads and observe the invasion morphology. The control parameters are the injection rate, the bead size, and the confining stress. We identify three invasion regimes: capillary fingering, viscous fingering, and "capillary fracturing", where capillary forces overcome frictional resistance and induce the opening of conduits (Fig. 10). We derive two dimensionless numbers that govern the transition among the different regimes: a modified capillary number and a fracturing number (Fig. 11). The experiments and analysis predict the emergence of fracturing in fine-grained media under low confining stress, a phenomenon that likely plays a fundamental role in many natural processes such as primary oil migration, methane venting from lake sediments, and the formation of desiccation cracks.

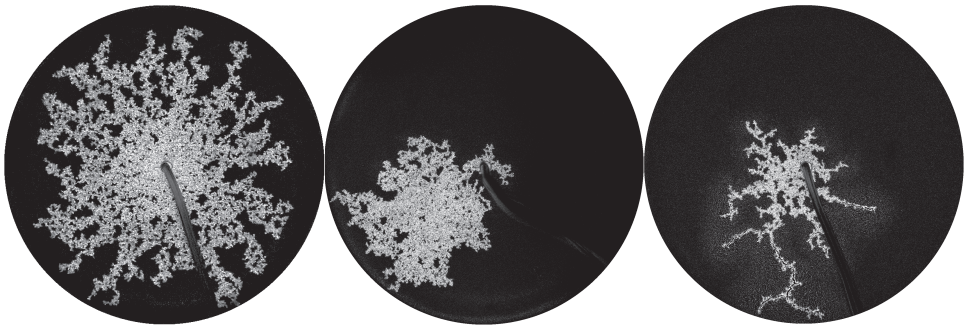

Figure 10. Examples of experimentally-observed patterns. We classify these patterns into three regimes: viscous fingering, capillary fingering, and fracturing. In these difference images, obtained by subtracting the initial image prior to air invasion, air shows as clear white, water and beads as black, and deformed regions as a sparkly halo (bead displacements changes the reflected light). Experimental conditions: d=360 μm; w=181 N (a, b) and 3 N (c); and q=100 (a), 0.1 (b), and 1 mL/min (c).

5.1.2 Three-dimensional simulation of unstable gravity-driven infiltration of water into a porous medium [9]

Infiltration of water in dry porous media is subject to a powerful gravity-driven instability. Although the phenomenon of unstable infiltration is well known, its description using continuum mathematical models has posed a significant challenge for several decades. The classical model of water flow in the unsaturated flow, the Richards equation, is unable to reproduce the instability. Here, we present a computational study of a model of unsaturated flow in porous media that extends the Richards equation and is capable of predicting the instability and captures the key features of gravity fingering quantitatively. The extended model is based on a phase-field formulation and is fourth-order in space. The new model poses a set of challenges for numerical discretizations, such as resolution of evolving interfaces, stiffness in space and time, treatment of singularly perturbed

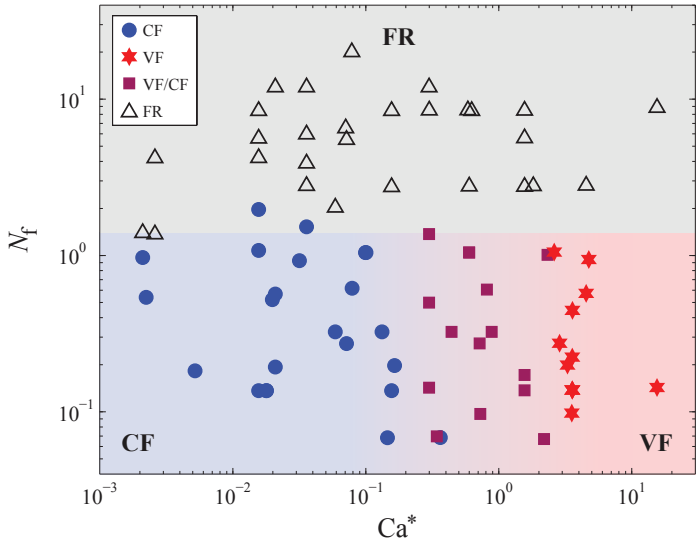

Figure 11. Phase diagram of drainage in granular media, showing three invasion regimes: viscous fingering (VF), capillary fingering (CF), and fracturing (FR). The dashed lines denote the approximate locations of the transitions among regimes. The tendency to fracture is characterized by the "fracturing number" N_f: drainage is dominated by fracturing in systems with $N_f \gg 1$. At lower N_f values, the type of fingering depends on the modified capillary number, Ca^*.

equations, and discretization of higher-order spatial partial-differential operators. We develop a numerical algorithm based on Isogeometric Analysis, a generalization of the finite element method that permits the use of globally-smooth basis functions, leading to a simple and efficient discretization of higher-order spatial operators in variational form. We illustrate the accuracy, efficiency and robustness of our method with several examples in two and three dimensions in both homogeneous and strongly heterogeneous media. We simulate, for the first time, unstable gravity-driven infiltration in three dimensions, and confirm that the new theory reproduces the fundamental features of water infiltration into a porous medium. Our results are consistent with classical experimental observations that demonstrate a transition from stable to unstable fronts depending on the infiltration flux (Fig. 12).

5.1.3 Stabilizing fluid-fluid displacements in porous media through wettability alteration [22]

We study experimentally how wettability impacts fluid–fluid displacement patterns in granular media. We inject a low-viscosity fluid (air) into a thin bed of glass beads initially saturated with a more-viscous fluid (a water/glycerol mixture). Chemical treatment of glass surfaces allows us to control the wetting properties of the medium and modify the contact angle θ from 5 deg (drainage) to 120 deg (imbibition). We demonstrate that wettability exerts a powerful influence on the invasion morphology of unfavorable-mobility displacements: increasing θ stabilizes fluid invasion into the granular pack at all capillary numbers. In particular, we report the striking observation of a stable radial displacement at low capillary numbers, whose origin lies on the cooperative nature of fluid invasion at the pore scale (Fig. 13).

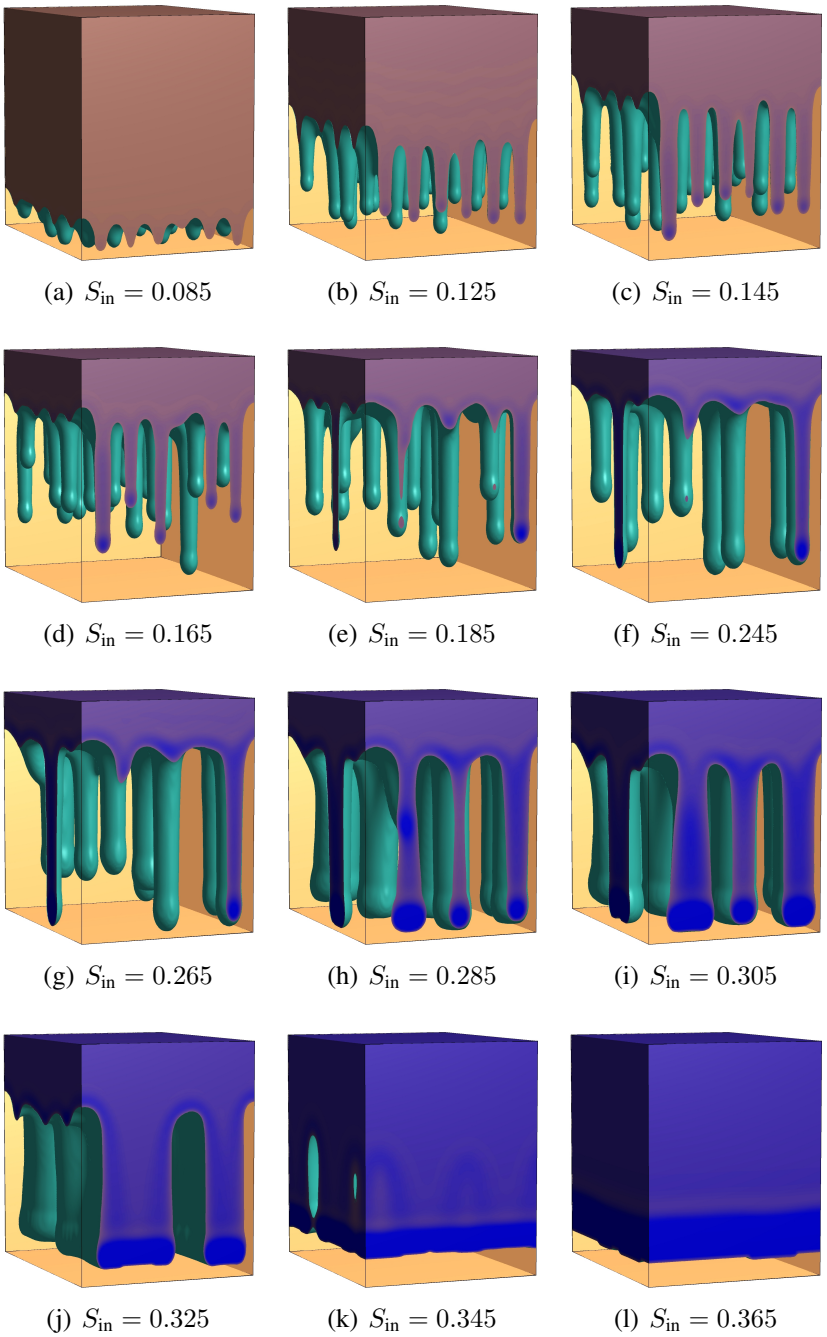

(a) $S_{\text{in}} = 0.085$ (b) $S_{\text{in}} = 0.125$ (c) $S_{\text{in}} = 0.145$

(d) $S_{\text{in}} = 0.165$ (e) $S_{\text{in}} = 0.185$ (f) $S_{\text{in}} = 0.245$

(g) $S_{\text{in}} = 0.265$ (h) $S_{\text{in}} = 0.285$ (i) $S_{\text{in}} = 0.305$

(j) $S_{\text{in}} = 0.325$ (k) $S_{\text{in}} = 0.345$ (l) $S_{\text{in}} = 0.365$

Figure 12. Three-dimensional simulations of water infiltration into a porous medium. The plots show isosurfaces of water saturation computed on a mesh of 128^3 quadratic elements. The flow is initialized with a perturbed flat wetting front at a distance 0.1 of the top of the domain. The wetting front moves downwards due to the action of gravity and capillarity, developing the so-called fingering instability for certain values of the infiltration ratio, which in our simulations is determined by the value of S_{in}. Each subfigure corresponds to a different value of S_{in}, as indicated in the labels that accompany the subplots.

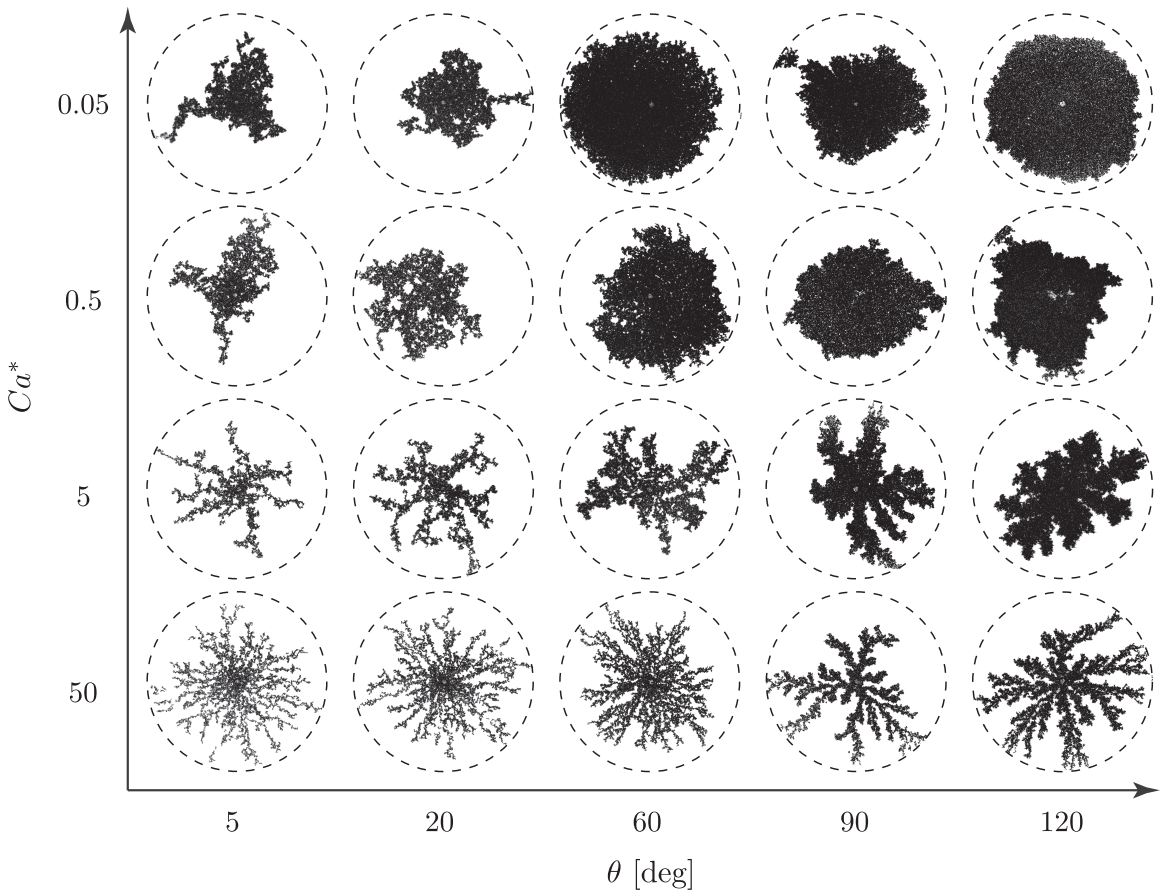

Figure 13. Visual phase diagram of the fluid-fluid displacement morphologies obtained during air injection (dark) into a porous medium filled with a mixture of water/glycerol (clear), as a function of the effective capillary number Ca^* and the static contact angle θ ranging from strict drainage ($\theta \approx 5$ deg) to forced imbibition ($\theta \approx 120$ deg). The viscosity contrast between the fluids is $M = \eta_{\text{liq}}/\eta_{\text{air}} \approx 320$.

5.2 Impact of heterogeneity

5.2.1 Impact of viscous fingering and permeability heterogeneity on fluid mixing in porous media [17]

Fluid mixing plays a fundamental role in many natural and engineered processes, including groundwater flows in porous media, enhanced oil recovery, and microfluidic lab-on-a-chip systems. Recent developments have explored the effect of viscosity contrast on mixing, suggesting that the unstable displacement of fluids with different viscosities, or viscous fingering, provides a powerful mechanism to increase fluid–fluid interfacial area and enhance mixing. However, existing studies have not incorporated the effect of medium heterogeneity on the mixing rate. Here, we characterize the evolution of mixing between two fluids of different viscosity in heterogeneous porous media. We focus on a practical scenario of divergent–convergent flow in a quarter five-spot geometry prototypical of well-driven groundwater flows. We study by means of numerical simulations the impact of permeability heterogeneity and viscosity contrast on the breakthrough curves and mixing efficiency, and we rationalize the nontrivial mixing behavior that emerges from the competition between the creation of fluid-fluid interfacial area and channeling.

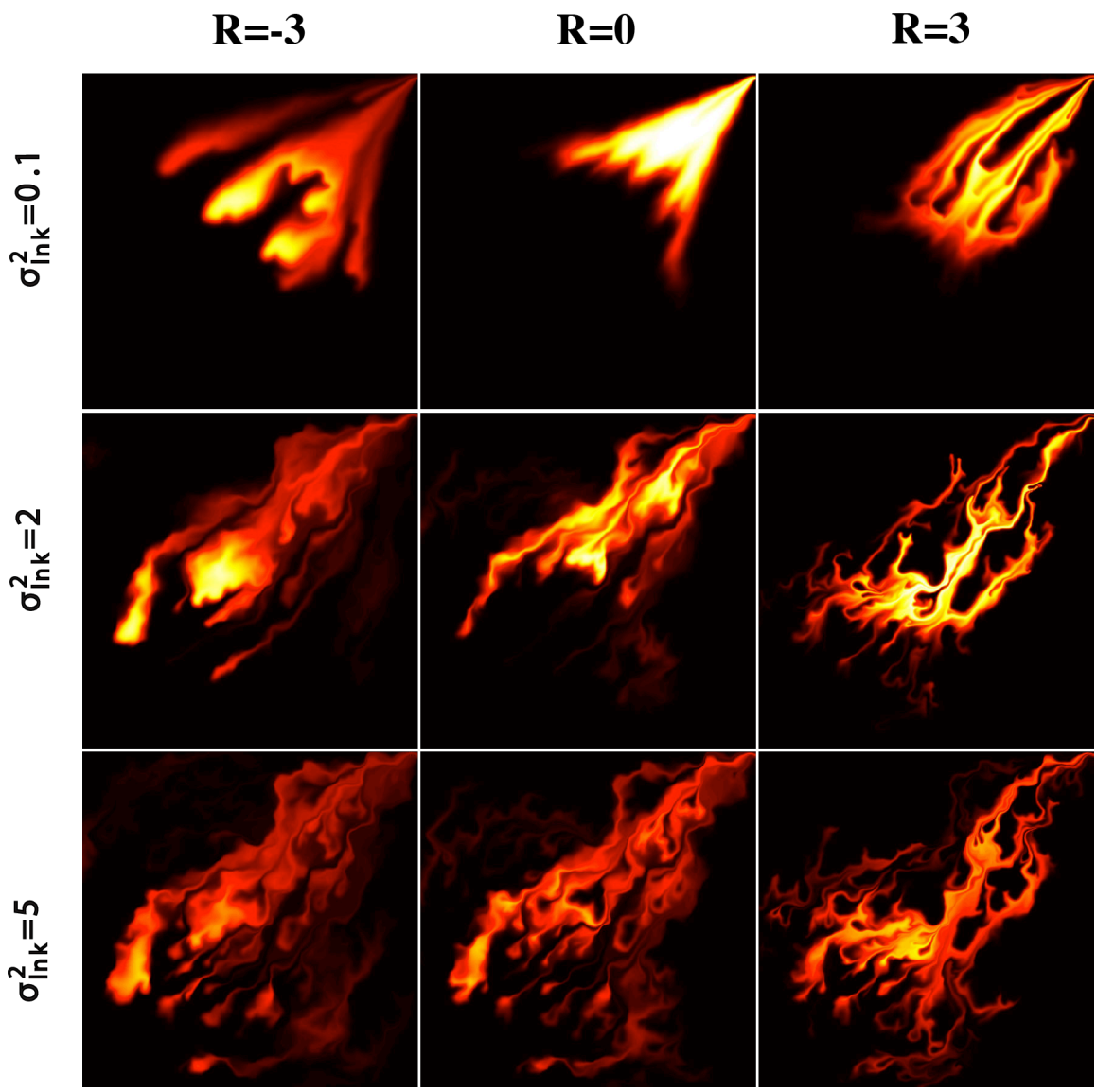

Figure 14. Snapshots of the contaminant concentration field at the time when 20% of the initial mass of contaminant fluid has been removed, for different viscosity contrasts (R) and for different levels of heterogeneity in the permeability field ($\sigma^2_{\ln k}$).

6 Application to CO_2 storage in saline aquifers

6.1 Capillary hysteresis

6.1.1 Interface pinning of immiscible gravity-exchange flows in porous media [23]

We study the gravity-exchange flow of two immiscible fluids in a porous medium and show that, in contrast with the miscible case, a portion of the initial interface remains pinned at all times (Fig. 15). We elucidate, by means of micromodel experiments, the pore-level mechanism responsible for capillary pinning at the macroscale. We propose a sharp-interface gravity-current model that incorporates capillarity and quantitatively explains the experimental observations, including the $x \sim t^{1/2}$ spreading behavior at intermediate times and the fact that capillarity stops a finite-release current. Our theory and experiments suggest that capillary pinning is potentially an important, yet unexplored, trapping mechanism during CO_2 sequestration in deep saline aquifers (Fig. 16).

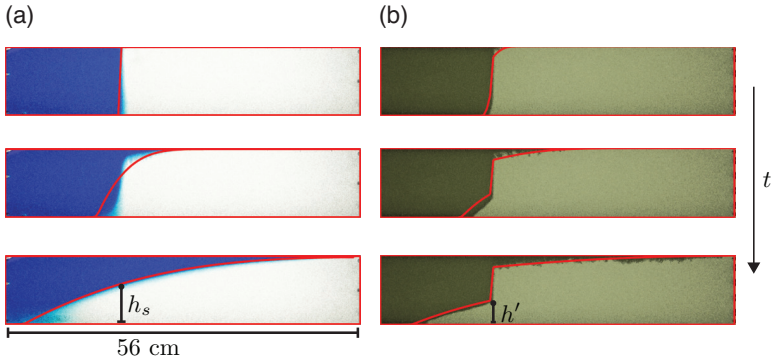

Figure 15. (Color online) Lock-exchange flow in a porous medium with (a) miscible and (b) immiscible fluids. (a) The miscible fluids are water (blue) spreading over a denser, more viscous mixture of glycerol and water. A smooth macroscopic interface tilts around a stationary point with fixed height h_s. (b) The immiscible fluids are air (dark) spreading over the same glycerol–water mixture. Part of the initial interface remains pinned, which leads to sharp kinks or "hinges" in the macroscopic interface. We denote the height of the lower hinge by h'. Both experiments were conducted in a transparent cell packed with 1 mm glass beads. The red curves correspond to the predictions of sharp-interface models.

6.1.2 A discrete-domain description of multiphase flow in porous media: Rugged energy landscapes and the origin of hysteresis [5]

We propose a discrete-domain model to describe mesoscale (many pore) immiscible displacements in porous media. We conceptualize the porous medium and fluid system as a set of weakly connected multistable compartments. The overall properties of the system emerge from the small-scale compartment dynamics. Our model aims at capturing the rugged energy landscape of multiphase porous media systems, emphasizing the role of metastability and local equilibria in the origin of hysteresis (Fig. 17). Under two-phase displacements, the system behaves hysteretically, but our description does not rely on past saturations, turning points, or drainage/imbibition labels. We characterize the connection between micrometastability and overall system behavior, and eluci-

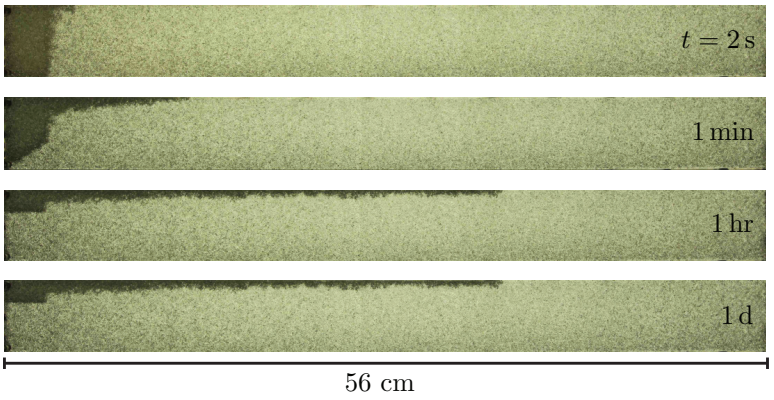

Figure 16. Finite release of a buoyant, nonwetting fluid (air) in a porous medium filled with a dense, wetting fluid (silicone oil). The dense, wetting front hits the left boundary, changing the spreading behavior of the buoyant current. Capillary hysteresis is responsible for the pinning of the initial interface and, ultimately, for stopping the buoyant plume at a finite distance, in stark contrast with a miscible plume which would continue to spread indefinitely.

date the different nature of pressure-controlled and rate-controlled immiscible displacements in porous media.

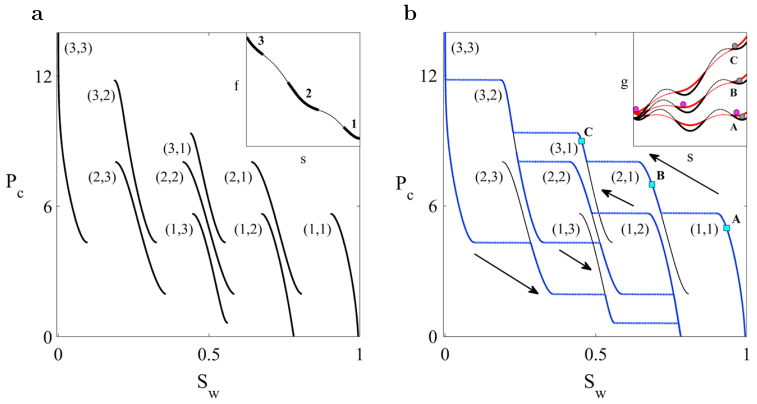

Figure 17. Hysteresis in pressure-controlled displacements. (a) Metastable branches for a two-compartment, three-well system. (b) We simulate two cycles of drainage and imbibition, illustrating the hysteretic behavior of the system. As we increase or decrease the capillary pressure, the P_c–S_w state follows reversible paths along metastable branches and jumps irreversibly among neighbor branches (blue line). (inset) For a given capillary pressure, compartment saturations relax toward minima of equation (3). A point in the P_c–S_w diagram is a combination of local equilibria at the compartments.

6.2 Dissolution and mixing

6.2.1 Scaling of convective mixing in porous media [10]

Convective mixing in porous media is triggered by a Rayleigh–Bénard-type hydrodynamic instability as a result of an unstable density stratification of fluids (Fig. 18). While convective mixing has been studied extensively, the fundamental behavior of the dissolution flux and its dependence

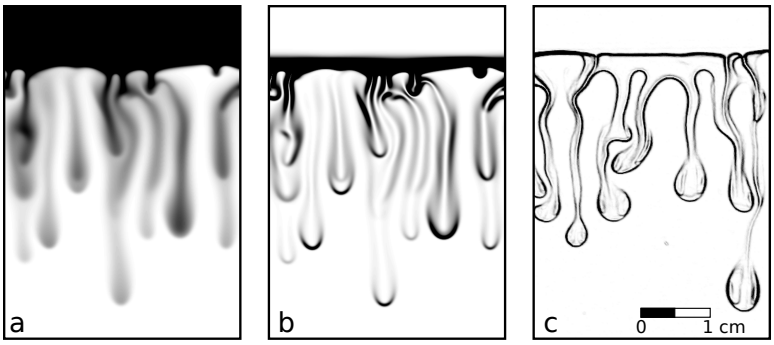

Figure 18. a, Snapshot of the concentration c at dimensionless time $t = 1$ from a simulation of the analogue-fluid system with Rayleigh number $\mathrm{Ra} = 10,000$ and constant viscosity ($R = 0$). A computational grid of 512×1536 cells was used, and only a small window of the simulation domain is shown. **b,** Corresponding snapshot of the scalar dissipation rate ϵ, for the same simulation as that in figure a. Here, dark color corresponds to high values of ϵ, and indicates regions of active mixing. **c,** Snapshot of a surrogate of the scalar dissipation rate $\epsilon = \nabla c \cdot D_m \nabla c$ (obtained from light intensity) from a laboratory experiment with a PG–water system in a Hele-Shaw cell, illustrating that mixing is primarily confined to narrow layers along the edges of the horizontal interface and the density-driven fingers.

on the system parameters are not yet well understood. Here, we show that the dissolution flux and the rate of fluid mixing are determined by the mean scalar dissipation rate. We use this theoretical result to provide computational evidence that the classical model of convective mixing in porous media exhibits, in the regime of high Rayleigh number, a dissolution flux that is constant and independent of the Rayleigh number. Our findings support the universal character of convective mixing and point to the need for alternative explanations for nonlinear scalings of the dissolution flux with the Rayleigh number, recently observed experimentally.

6.2.2 The evolution of miscible gravity currents in horizontal porous layers [19]

Gravity currents of miscible fluids in porous media are important to understand because they occur in important engineering projects, such as enhanced oil recovery and geologic CO_2 sequestration. These flows are often modeled based on two simplifying assumptions: vertical velocities are negligible compared to horizontal velocities, and diffusion is negligible compared to advection. In many cases, however, these assumptions limit the validity of the models to a finite, intermediate time interval during the flow, making prediction of the flow at early and late times difficult. Here, we consider the effects of vertical flow and diffusion to develop a set of models for the entire evolution of a miscible gravity current. To gain physical insight, we study a simple system: lock exchange of equal-viscosity fluids in a horizontal, vertically-confined layer of permeable rock. We show that the flow exhibits five regimes: 1. an early-diffusion regime, in which the fluids diffuse across the initially sharp fluid-fluid interface; 2. an S-slumping regime, in which the fluid-fluid interface tilts in an S-shape; 3. a straight-line slumping regime, in which the fluid-fluid interface tilts as a straight line; 4. a Taylor-slumping regime, in which Taylor dispersion at the aquifer scale enhances mixing between the fluids and causes the flow to continuously decelerate; and 5. a late-diffusion regime, in which the flow becomes so slow that mass transfer again occurs dominantly though diffusion (Fig. 19).

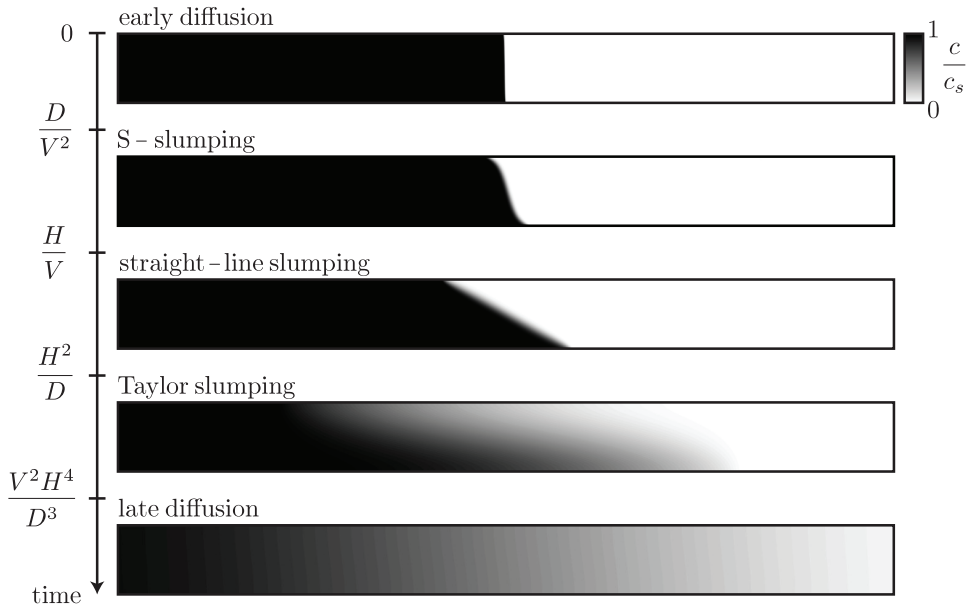

Figure 19. The flow evolves through the five self-similar regimes shown here by simulation results. The grey scale represents the concentration of the more dense fluid, c, normalized to the saturated concentration, c_s. The scalings of the transition times between the regimes are shown in terms of the layer thickness, H, the diffusion coefficient, D, and the characteristic velocity, $V = \Delta\rho g k/\mu\phi$. When $HV/D \lesssim 1$, the first and final transition times become equal, the duration of the intermediate regimes becomes zero, and lateral diffusion becomes the dominant mass transfer mechanism for all times.

6.2.3 Pattern formation and coarsening dynamics in three-dimensional convective mixing in porous media [6]

Geologic carbon dioxide sequestration entails capturing and injecting CO_2 into deep saline aquifers for long-term storage. The injected CO_2 partially dissolves in groundwater to form a mixture that is denser than the initial groundwater. The local increase in density triggers a gravitational instability at the boundary layer that further develops into columnar plumes of CO_2-rich brine, a process that greatly accelerates solubility trapping of the CO_2. Here, we investigate the pattern-formation aspects of convective mixing during geological CO_2 sequestration by means of high-resolution three-dimensional simulation (Fig. 20). We find that the CO_2 concentration field self-organizes as a cellular network structure in the diffusive boundary layer at the top boundary. By studying the statistics of the cellular network, we identify various regimes of finger coarsening over time, the existence of a nonequilibrium stationary state, and a universal scaling of 3D convective mixing.

6.2.4 Rock dissolution patterns and geochemical shutdown of CO_2-brine-carbonate reactions during convective mixing in porous media [7]

Motivated by the process of CO_2 convective mixing in porous media, here we study the formation of rock-dissolution patterns that arise from geochemical reactions during Rayleigh–Bénard–Darcy convection. Under the assumption of instantaneous chemical equilibrium, we adopt a formulation of the local reaction rate as a function of scalar dissipation rate—a measure that depends solely on flow and transport—and chemical speciation, which is a measure that depends only on the equilib-

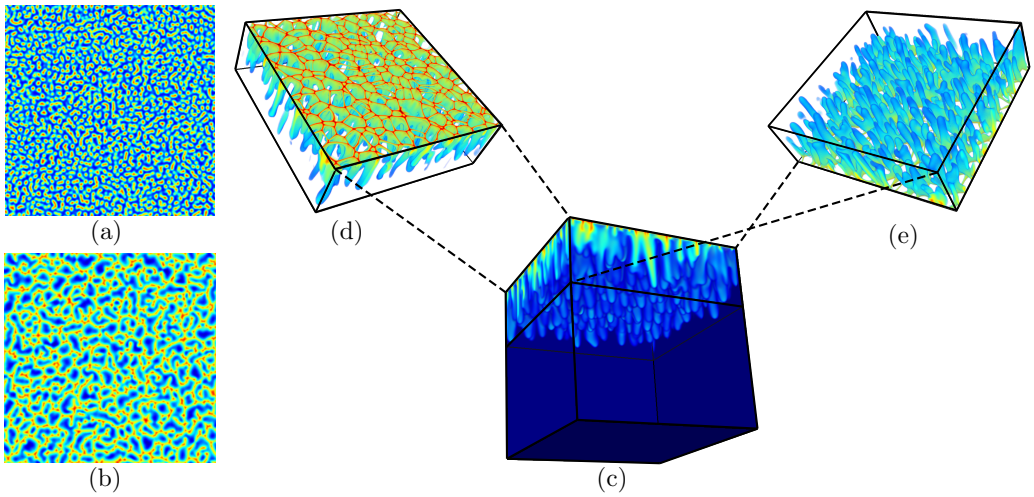

Figure 20. Simulation of convective mixing with Ra $= 6400$ on a 512^3 grid. (a) Snapshot of the concentration field at a slice near the top boundary ($z = 0.01$) at $t = 0.5$, showing a pattern of disconnected islands of high concentration. (b) Snapshot of the same slice at $t = 1$, showing a partially-connected maze structure. (c)-(e) Snapshot of the 3D concentration field at $t = 2$; (c) is a complete view of the computational domain; (d) is a view of a partial volume ($0.01 < z < 0.3$) from the top, illustrating the celular network structure that emerges at the boundary layer; (e) is a view of the same volume from the bottom, illustrating the columnar pattern of CO_2-rich fingers that sink away from the top boundary.

rium thermodynamics of the chemical system. We use high-resolution simulations to examine the interplay between the density-driven hydrodynamic instability and the rock dissolution reactions, and analyze the impact of geochemical reactions on the macroscopic mass exchange rate. We find that dissolution of carbonate rock initiates in regions of locally high mixing, but that the geochemical reaction shuts down significantly earlier than shutdown of convective mixing. This early shutdown feature reflects the important role that chemical speciation plays in this hydrodynamics–reaction coupled process. Finally, we extend our analysis to three dimensions and explore the morphology of dissolution patterns in 3D (Fig. 21).

6.3 CO_2 migration and storage efficiency

6.3.1 Lifetime of carbon capture and storage as a climate-change mitigation technology [20]

In carbon capture and storage (CCS), CO_2 is captured at power plants and then injected underground into reservoirs like deep saline aquifers for long-term storage (Fig. 22). While CCS may be critical for the continued use of fossil fuels in a carbon-constrained world, the deployment of CCS has been hindered by uncertainty in geologic storage capacities and sustainable injection rates, which has contributed to the absence of concerted government policy. Here, we clarify the potential of CCS to mitigate emissions in the US by developing a storage-capacity supply curve that, unlike current large-scale capacity estimates, is derived from the fluid mechanics of CO_2 injection and trapping, and incorporates injection-rate constraints. We show that storage supply is a dynamic quantity that grows with the duration of CCS, and we interpret the lifetime of CCS as the time for

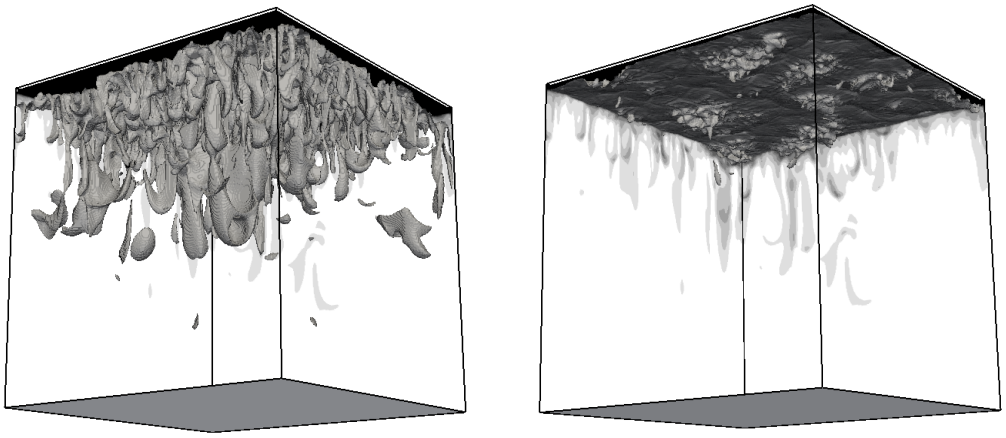

Figure 21. Rock dissolution patterns in 3D as a result of CO_2 convective mixing, for a simulation with H=2500, Da=5 and R_ϕ=2, at $t/H = 14.0$, this figure shows surface contours for (a) $\Delta\phi = 4\%$ and (b) $\Delta\phi = 8\%$.

which the storage supply curve exceeds the storage demand curve from CO_2 production. We show that in the US, if CO_2 production from power generation continues to rise at recent rates, then CCS can store enough CO_2 to stabilize emissions at current levels for at least 100 years (Fig. 23). This result suggests that the large-scale implementation of CCS is a geologically-viable climate-change mitigation option in the US over the next century.

6.3.2 Buoyant currents arrested by convective dissolution [16]

When carbon dioxide (CO_2) dissolves into water, the density of water increases. This seemingly insubstantial phenomenon has profound implications for geologic carbon sequestration. Here we show, by means of laboratory experiments with analogue fluids, that the up-slope migration of a buoyant current of CO_2 is arrested by the convective dissolution that ensues from a fingering instability at the moving CO_2–groundwater interface (Fig. 24). We consider the effectiveness of convective dissolution as a large-scale trapping mechanism in sloping aquifers, and we show that a small amount of slope is beneficial compared to the horizontal case. We study the development and coarsening of the fingering instability along the migrating current, and predict the maximum migration distance of the current with a simple sharp-interface model. We show that convective dissolution exerts a powerful control on CO_2 plume dynamics and, as a result, on the potential of geologic carbon sequestration.

6.3.3 Dynamics of convective dissolution from a migrating current of carbon dioxide [11]

During geologic storage of carbon dioxide (CO_2), trapping of the buoyant CO_2 after injection is essential in order to minimize the risk of leakage into shallower formations through a fracture or abandoned well. Models for the subsurface behavior of the CO_2 are useful for the design, implementation, and long-term monitoring of injection sites, but traditional reservoir-simulation tools are currently unable to resolve the impact of small-scale trapping processes on fluid flow at the

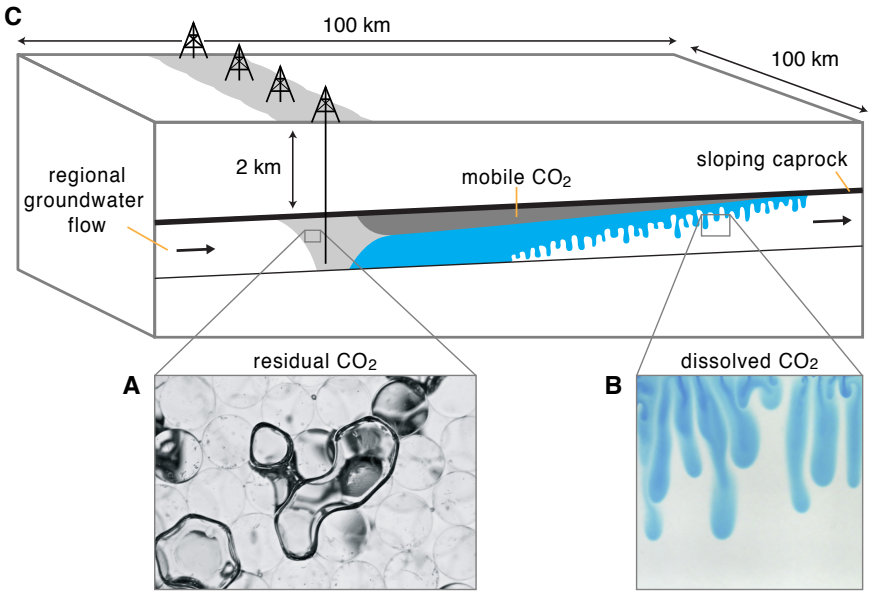

Figure 22. Residual and solubility trapping are the key trapping mechanisms that contribute to the CO_2 storage capacity. Inset (**A**) shows blobs of gas immobilized by residual trapping in an experimental analog system: a glass-bead pack saturated with water. Inset (**B**) shows solubility trapping in a different analog system: a Hele-Shaw cell saturated with water, topped with a source of dense, dyed water. As in the CO_2 system, in which the brine with dissolved CO_2 is denser than the ambient brine, dissolution occurs via finger-like protrusions of dense fluid. (**C**) We model trapping at the large scales relevant to a nationwide analysis, and account for the injection and migration of CO_2. We consider a linear arrangement of injection wells in a deep section of the aquifer. Initially, each well produces a radial CO_2 plume, which grows and eventually interferes with those from neighboring wells, leading to a problem that can be approximated as two-dimensional on a vertical cross section. Trapping occurs primarily after injection, when the CO_2 migrates due to the aquifer slope and the natural head gradient. As the buoyant CO_2 plume rises and spreads away from the well array (dark gray), residual trapping immobilizes blobs of CO_2 in its wake (light gray), and solubility trapping shrinks the plume from below (blue).

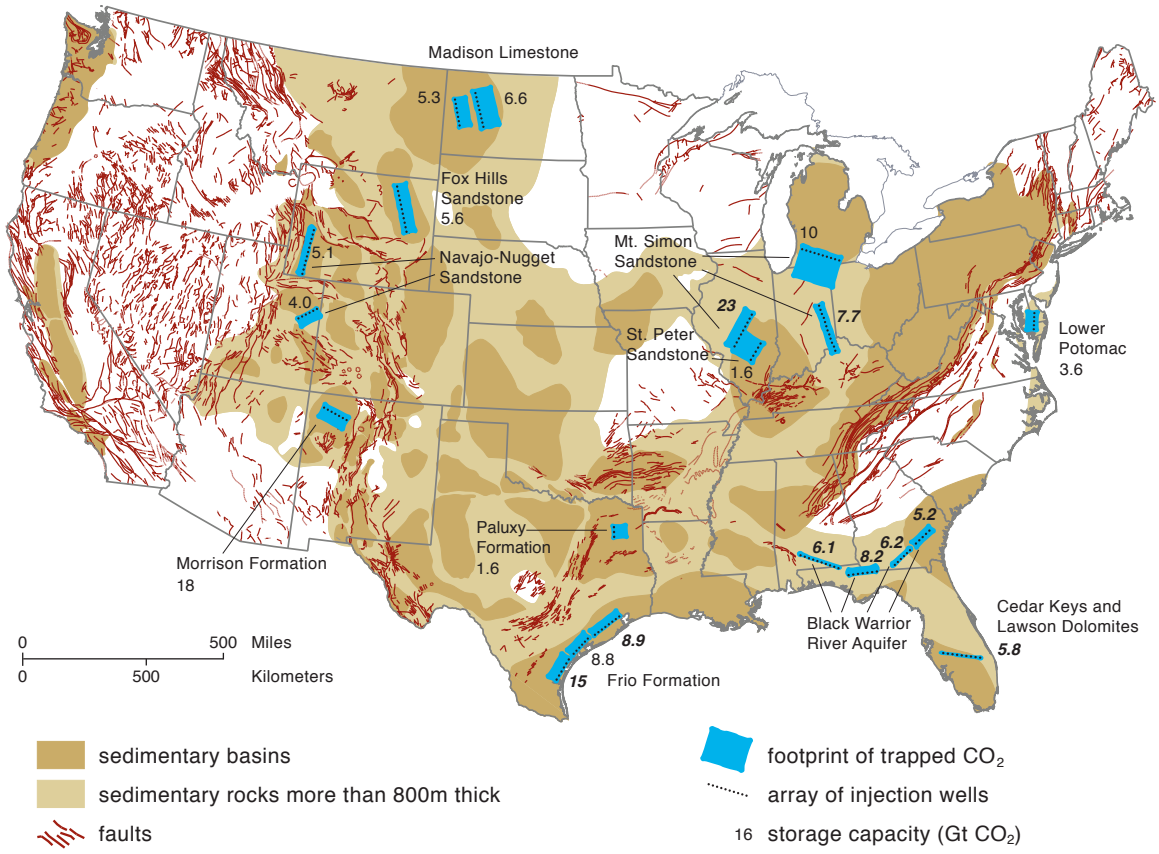

Figure 23. We estimate the nationwide storage capacity from 20 arrays of injection wells in 11 aquifers. We select these aquifers because they are large, exhibit few basin-scale faults, and have been relatively well characterized. This map shows the locations of the aquifers and their storage capacities for an injection period of 100 years (capacities for different injection periods are in Table S29). Capacities in boldface italics are constrained by pressure; otherwise, they are constrained by migration. The map also shows the ultimate CO_2 footprints for those capacities, which correspond to the areas infiltrated by migrating, free-phase CO_2 before it becomes completely trapped.

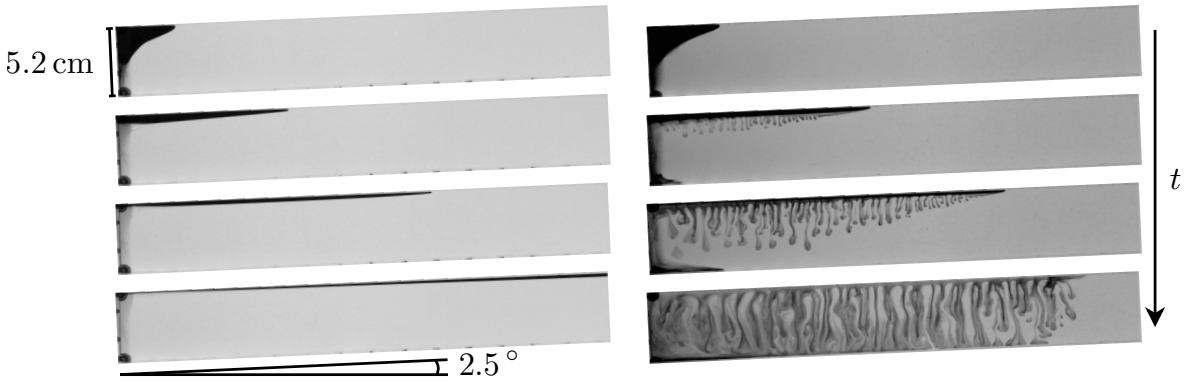

Figure 24. Convective dissolution arrests the up-slope migration of a buoyant current. Here we show snapshots of two buoyant currents migrating up-slope in a sloping aquifer (a Hele-Shaw cell for illustration). The CO_2 analogue is water (dark) in both cases. When the denser and more viscous ambient fluid is a mixture of glycerol and water (left), the fluids mix by diffusion-dispersion only and the buoyant current migrates to the top of the cell and accumulates there. When the ambient fluid is propylene glycol (right), the dense mixture of the two fluids drives convective dissolution, which dissolves the buoyant current as it migrates.

scale of a geologic basin. Here, we study the impact of solubility trapping from convective dissolution on the up-dip migration of a buoyant gravity current in a sloping aquifer. To do so, we conduct high-resolution numerical simulations of the gravity current that forms from a pair of miscible analogue fluids. Our simulations fully resolve the dense, sinking fingers that drive the convective dissolution process (Fig. 25). We analyze the dynamics of the dissolution flux along the moving CO_2–brine interface, including its decay as dissolved buoyant fluid accumulates beneath the buoyant current. We show that the dynamics of the dissolution flux and the macroscopic features of the migrating current can be captured with an upscaled sharp-interface model.

Figure 25. Sequence of snapshots from a high-resolution simulation of convective dissolution from a buoyant current in a sloping aquifer for Ra $= 5000$, $R = 1$, and $\theta = 2.5°$ (not shown) at dimensionless times 0, 3, 9, and 27. The domain extends to $x = 20$, but only $0 \leq x \leq 15$ is shown here. The red line marks the contour of neutrally buoyant concentration $c = c_n$, which separates the buoyant current from the sinking fluid.

6.3.4 Carbon dioxide dissolution in structural and stratigraphic traps [21]

The geologic sequestration of carbon dioxide (CO_2) in structural and stratigraphic traps is a viable option to reduce anthropogenic emissions. While dissolution of the CO_2 stored in these traps reduces the long-term leakage risk, the dissolution process remains poorly understood in systems that reflect the appropriate subsurface geometry. Here, we study dissolution in a porous layer that exhibits a feature relevant for CO_2 storage in structural and stratigraphic traps: a finite CO_2 source along the top boundary that extends only part way into the layer. This feature represents the finite extent of the interface between free-phase CO_2 pooled in a trap and the underlying brine. Using theory and simulations, we describe the dissolution mechanisms in this system for a wide range of times and Rayleigh numbers, and classify the behavior into seven regimes (Fig. 26). For each regime, we quantify the dissolution flux numerically and model it analytically, with the goal of providing simple expressions to estimate the dissolution rate in real systems. We find that, at late times, the dissolution flux decreases relative to early times as the flow of unsaturated water to the CO_2 source becomes constrained by a lateral exchange flow though the reservoir. Application of the models to several representative reservoirs indicates that dissolution is strongly affected by the reservoir properties; however, we find that reservoirs with high permeabilities ($k \geq 1$ Darcy) that are tens of meters thick and several kilometers wide could potentially dissolve hundreds of megatons of CO_2 in tens of years.

6.3.5 Capillary pinning and blunting of immiscible gravity currents in porous media [24]

Gravity-driven flows in the subsurface have attracted recent interest in the context of geological carbon dioxide (CO_2) storage, where supercritical CO_2 is captured from the flue gas of power plants and injected underground into deep saline aquifers. After injection, the CO_2 will spread and migrate as a buoyant gravity current relative to the denser, ambient brine. Although the CO_2 and the brine are immiscible, the impact of capillarity on CO_2 spreading and migration is poorly understood. We previously studied the early-time evolution of an immiscible gravity current, showing that capillary pressure hysteresis pins a portion of the macroscopic fluid-fluid interface and that this can eventually stop the flow. Here, we study the full lifetime of such a gravity current. Using table-top experiments in packings of glass beads, we show that the horizontal extent of the pinned region grows with time, and that this is ultimately responsible for limiting the migration of the current to a finite distance (Fig. 27). We also find that capillarity blunts the leading edge of the current, which contributes to further limiting the migration distance. Using experiments in etched micromodels, we show that the thickness of the blunted nose is controlled by the distribution of pore-throat sizes and the strength of capillarity relative to buoyancy. We develop a theoretical model that captures the evolution of immiscible gravity currents and predicts the maximum migration distance. By applying this model to representative aquifers, we show that capillary pinning and blunting can exert an important control on gravity currents in the context of geological CO_2 storage.

6.3.6 Residual trapping, solubility trapping and capillary pinning complement each other to limit CO_2 migration in deep saline aquifers [25]

We derive a theoretical model for the post-injection migration of a CO_2 gravity current in a confined, sloping aquifer under the influence of residual trapping, solubility trapping, and capillary pinning. The resulting model consists of two coupled partial differential equations that describe

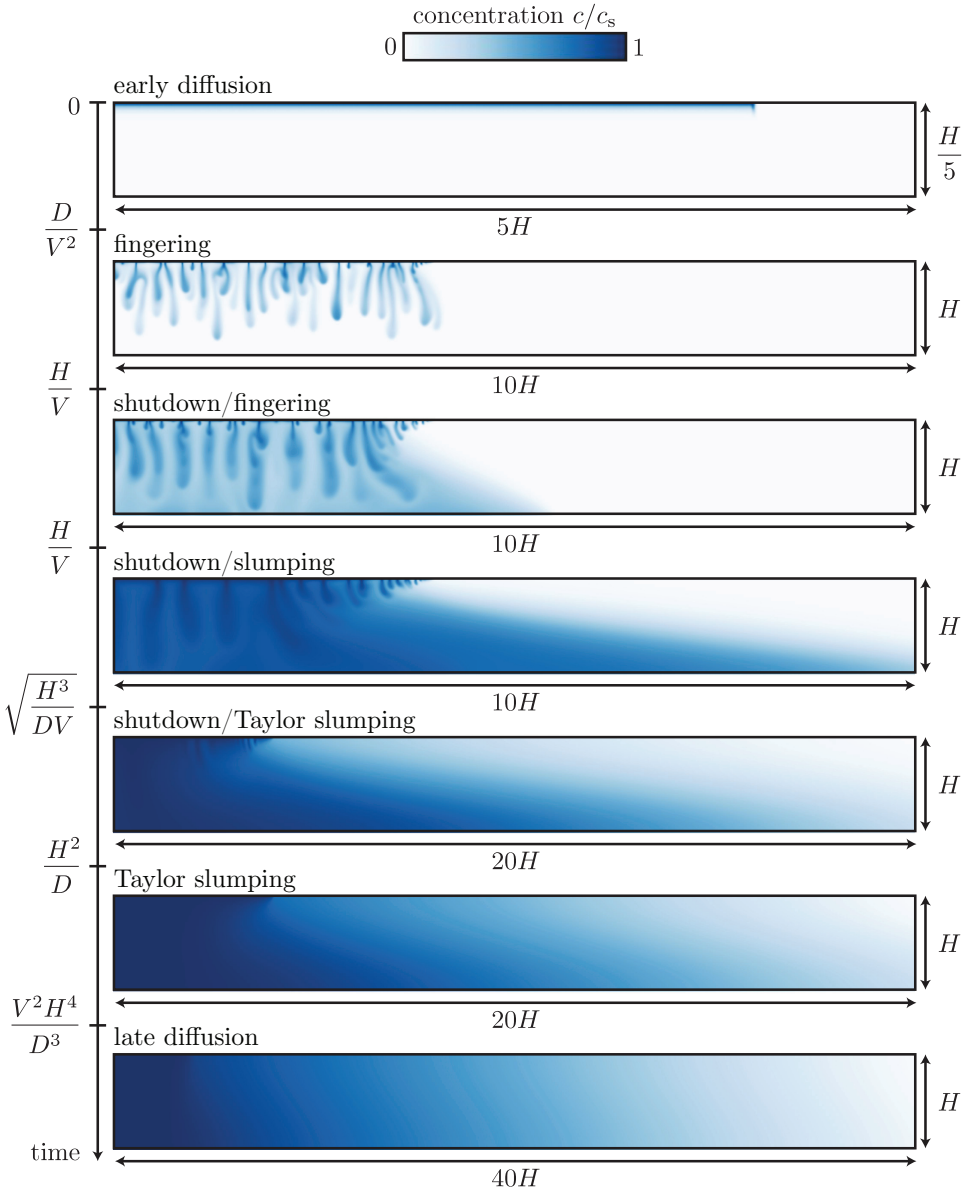

Figure 26. Dissolution evolves through the seven regimes shown here ($Ra = 3000$). The color scale represents the concentration of CO_2, c, normalized to the saturated concentration, c_s. The scalings of the transition times between the regimes are shown in terms of the layer thickness, H, the effective diffusion coefficient, D, and the characteristic velocity, $V = \Delta\rho g k/\mu\phi$. When $Ra = VH/D$ is sufficiently small, the first and final transition times become equal, the duration of the intermediate regimes becomes zero, and the system transitions directly to the late diffusion regime.

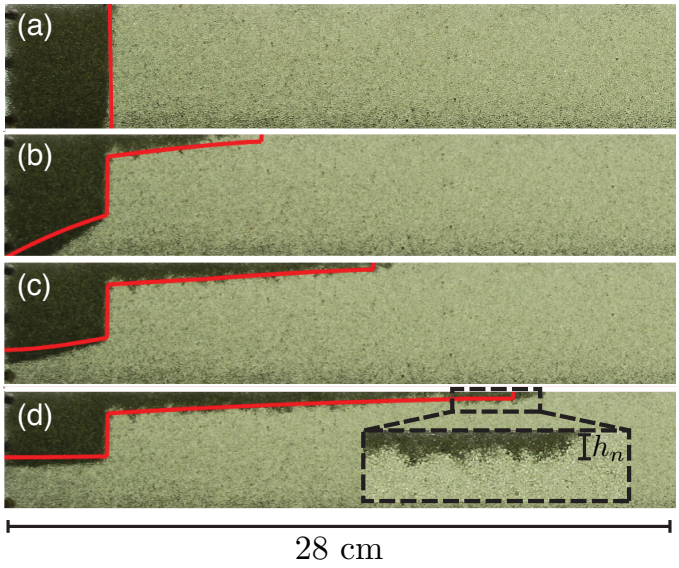

Figure 27. Gravity driven flow of a buoyant, nonwetting fluid (air) over a dense, wetting fluid (propylene glycol) in a packing of glass beads. (a-b) Starting with a vertical interface between the fluids, the flow first undergoes a lock-exchange process. (c-d) The process models a finite-release problem after the dense fluid reaches the left boundary. In contrast to the finite release of a miscible current that spreads indefinitely, spreading of an immiscible current stops at a finite distance. Dashed black box highlights the blunt nose of the current, which has thickness h_n. Red lines represent predictions from our macroscopic sharp-interface model.

the local thickness of the buoyant CO_2 current and the thickness of the mound of brine saturated with dissolved CO_2 as a function of time. We apply this model to a representative geological formation and provide estimates of the lifetime of the buoyant CO_2 current and its maximum migration distance. Our analysis shows that residual trapping, solubility trapping, and capillary pinning complement each other in limiting the ultimate migration distance of CO_2 gravity currents. The relative contribution of residual trapping, solubility trapping, and capillary pinning varies as a function of the injection volume. Our model can be used as a screening tool to evaluate the potential of deep saline aquifers for large-scale CO_2 sequestration.

7 Journal publications

[1] A. Alizadeh Pahlavan, L. Cueto-Felgueroso, and R. Juanes. Thin films in partial wetting: internal selection of contact-line dynamics. *Phys. Rev. Lett.*, 115:034502, doi:10.1103/PhysRevLett.115.034502, 2015.

[2] J. Y. Y. Chui, P. de Anna, and R. Juanes. Interface evolution during radial miscible viscous fingering. *Phys. Rev. E*, 92:041003(R), doi:10.1103/PhysRevE.92.041003, 2015.

[3] L. Cueto-Felgueroso and R. Juanes. Macroscopic phase-field modeling of partial wetting: bubbles in a capillary tube. *Phys. Rev. Lett.*, 108:144502, doi:10.1103/PhysRevLett.108.144502, 2012.

[4] L. Cueto-Felgueroso and R. Juanes. A phase-field model of two-phase Hele-Shaw flow. *J. Fluid Mech.*, 758:522–552, doi:10.1017/jfm.2014.512, 2014.

[5] L. Cueto-Felgueroso and R. Juanes. A discrete-domain description of multiphase flow in porous media: Rugged energy landscapes and the origin of hysteresis. *Geophys. Res. Lett.*, 43(4):1615–1622, doi:10.1002/2015GL067015, 2016.

[6] X. Fu, L. Cueto-Felgueroso, and R. Juanes. Pattern formation and coarsening dynamics in three-dimensional convective mixing in porous media. *Phil. Trans. R. Soc. A*, 371:20120355, doi:10.1098/rsta.2012.0355, 2013.

[7] X. Fu, L. Cueto-Felgueroso, D. Bolster, and R. Juanes. Rock dissolution patterns and geochemical shutdown of CO_2-brine-carbonate reactions during convective mixing in porous media. *J. Fluid Mech.*, 764:296–315, doi:10.1017/jfm.2014.647, 2015.

[8] X. Fu, L. Cueto-Felgueroso, and R. Juanes. Thermodynamic coarsening arrested by viscous fingering in partially-miscible binary mixtures. *Phys. Rev. E*, 94:033111, doi:10.1103/PhysRevE.94.033111, 2016.

[9] H. Gomez, L. Cueto-Felgueroso, and R. Juanes. Three-dimensional simulation of unstable gravity-driven infiltration of water into a porous medium. *J. Comput. Phys.*, 238:217–239, doi:10.1016/j.jcp.2012.12.018, 2013.

[10] J. J. Hidalgo, J. Fe, L. Cueto-Felgueroso, and R. Juanes. Scaling of convective mixing in porous media. *Phys. Rev. Lett.*, 109:264503, doi:10.1103/PhysRevLett.109.264503, 2012.

[11] J. J. Hidalgo, C. W. MacMinn, and R. Juanes. Dynamics of convective dissolution from a migrating current of carbon dioxide. *Adv. Water Resour.*, 62:511–519, doi:10.1016/j.advwatres.2013.06.013, 2013.

[12] R. Holtzman, M. L. Szulczewski, and R. Juanes. Capillary fracturing in granular media. *Phys. Rev. Lett.*, 108:264504, doi:10.1103/PhysRevLett.108.264504, 2012.

[13] B. Jha, L. Cueto-Felgueroso, and R. Juanes. Quantifying mixing in viscously unstable porous media flows. *Phys. Rev. E*, 84:066312, doi:10.1103/PhysRevE.84.066312, 2011.

[14] B. Jha, L. Cueto-Felgueroso, and R. Juanes. Fluid mixing from viscous fingering. *Phys. Rev. Lett.*, 106:194502, doi:10.1103/PhysRevLett.106.194502, 2011.

[15] B. Jha, L. Cueto-Felgueroso, and R. Juanes. Synergetic fluid mixing from viscous fingering and alternating injection. *Phys. Rev. Lett.*, 111:144501, doi:10.1103/PhysRevLett.111.144501, 2013.

[16] C. W. MacMinn and R. Juanes. Buoyant currents arrested by convective dissolution. *Geophys. Res. Lett.*, 40:2017–2022, doi:10.1002/grl.50473, 2013.

[17] C. Nicolaides, B. Jha, L. Cueto-Felgueroso, and R. Juanes. Impact of viscous fingering and permeability heterogeneity on fluid mixing in porous media. *Water Resour. Res.*, 51(4):2634–2647, doi:10.1002/2014WR015811, 2015.

[18] M. Strait, M. Shearer, R. Levy, L. Cueto-Felgueroso, and R. Juanes. Two fluid flow in a capillary tube. *Springer Proceedings in Mathematics & Statistics*, 109:149–161, 2015.

[19] M. L. Szulczewski and R. Juanes. The evolution of miscible gravity currents in horizontal porous layers. *J. Fluid Mech.*, 719:82–96, doi:10.1017/jfm.2012.631, 2013.

[20] M. L. Szulczewski, C. W. MacMinn, H. J. Herzog, and R. Juanes. Lifetime of carbon capture and storage as a climate-change mitigation technology. *Proc. Natl. Acad. Sci. U.S.A.*, 109 (14):5185–5189, doi:10.1073/pnas.1115347109, 2012.

[21] M. L. Szulczewski, M. A. Hesse, and R. Juanes. Carbon dioxide dissolution in structural and stratigraphic traps. *J. Fluid Mech.*, 736:287–315, doi:10.1017/jfm.2013.511, 2013.

[22] M. Trojer, M. L. Szulczewski, and R. Juanes. Stabilizing fluid-fluid displacements in porous media through wettability alteration. *Phys. Rev. Applied*, 3:054008, doi:10.1103/PhysRevApplied.3.054008, 2015.

[23] B. Zhao, C. W. MacMinn, M. L. Szulczewski, J. A. Neufeld, H. E. Huppert, and R. Juanes. Interface pinning of immiscible gravity-exchange flows in porous media. *Phys. Rev. E*, 87: 023015, doi:10.1103/PhysRevE.87.023015, 2013.

[24] B. Zhao, C. W. MacMinn, H. E. Huppert, and R. Juanes. Capillary pinning and blunting of immiscible gravity currents in porous media. *Water Resour. Res.*, 50(9):7067–7081, doi:10.1002/2014WR015335, 2014.

[25] B. Zhao, C. W. MacMinn, and R. Juanes. Residual trapping, solubility trapping and capillary pinning complement each other to limit CO2 migration in deep saline aquifers. *Water Resour. Res.*, 63:3833–3839, 2014.

[26] B. Zhao, C. W. MacMinn, and R. Juanes. Wettability control on multiphase flow in patterned microfluidics. *Proc. Natl. Acad. Sci. U.S.A.*, 111(37):10251–10256, doi:10.1073/pnas.1603387113, 2016.

8 Selected invited lectures and talks

07/2016 Frontiers of Geoscience Colloquium, Computational modeling of induced seismicity, Los Alamos National Laboratory, Los Alamos, NM.

06/2016 Plenary speaker, Computational modeling of induced seismicity, Computational Methods in Water Resources Conference — CMWR 2016, Toronto

05/2016 Gravity fingering during water infiltration and potential implications for the ecohydrology of arid climates, Princeton University, Princeton, NJ.

02/2016 Computational modeling of induced seismicity, Harvard University, Cambridge, MA

12/2015 Invited talk, Fracturing in granular media: the role of capillarity, wetting, and disorder, American Geophysical Union (AGU) Fall Meeting, San Francisco, CA.

11/2015 Invited talk, Fracturing in granular media: the role of capillarity, wetting, and disorder, American Physical Society (APS) Division of Fluid Dynamics Meeting, Boston, MA.

11/2015 Computational modeling of induced seismicity, Northeastern University, Boston, MA

09/2015 Plenary keynote speaker, Computational modeling of induced seismicity, TOUGH Symposium, Lawrence Berkeley National Lab, Berkeley, CA.

09/2015 Hydro-capillary fracking: understanding and controlling capillary and wetting effects on fracturing of granular media, Geological Fluid Mechanics Workshop, Santa Fe, NM.

07/2015 Invited lecture, Cargése Summer School on Flow and Transport in Porous and Fractured Media, Corsica, France.

06/2015 Plenary lecture, Computational modeling of induced seismicity, Engineering Mechanics Institute Conference — EMI 2015, Stanford.

05/2015 Invited talk, Computational modeling of coupled multiphase flow and geomechanics to study fault slip and induced seismicity, SIAM Geosciences Conference, Stanford.

04/2015 Computational modeling of coupled multiphase flow and geomechanics to study fault slip and induced seismicity, Penn State University.

03/2015 Plenary lecture, Fundamentals of multiphase flow in enhanced oil recovery, Offshore Mediterranean Conference — OMC 2015, Ravenna, Italy.

02/2015 Fingering, fracturing and dissolution in granular media, Department of Civil and Environmental Engineering and Earth Sciences, U. of Notre Dame.

01/2015 Computational modeling of coupled multiphase flow and geomechanics to study fault slip and induced seismicity, Department of Geophysics, Stanford University.

01/2015 Computational modeling of coupled multiphase flow and geomechanics to study fault slip and induced seismicity, Lawrence Livermore National Laboratory.

12/2014 Invited talk, A Computational Model of Coupled Multiphase Flow and Geomechanics to Study Fault Slip and Induced Seismicity, AGU Fall Meeting, San Francisco, CA.

11/2014 Fingering, fracturing and dissolution in porous media, Eindhoven Multiscale Institute, Eindhoven, The Netherlands.

10/2014 Fingering, fracturing and dissolution in granular media, Department of Petroleum Engineering, Texas A&M University.

02/2014 Invited lecture, Pattern formation and interface pinning in gravity-driven unsaturated flow through porous media: simulation and micromodel experiments, International Meeting on Dynamic Capillary Fringes — DyCap 2014, Karlsruhe, Germany.

01/2014 Fingering and fracturing in porous media, Department of Petroleum Engineering, Montanuniversitäet Leoben, Austria.

12/2013 Invited talk, Fingering and fracturing during multiphase flow in porous media, AGU Fall Meeting, San Francisco, CA.

11/2013 Lifetime of carbon capture and storage as a climate change mitigation technology, MIT-Total Symposium, Cambridge, MA.

06/2013 Invited talk, Lifetime of carbon capture and storage as a climate change mitigation technology, SIAM Geosciences Conference, Padova, Italy.

05/2013 Invited talk, Fingering and fracturing in granular media, InterPore 2013, Prague, Czech Republic.

05/2013 Nonequilibrium physics and phase-field modeling of multiphase flow in porous media, Department of Civil, Environmental and Geomatic Engineering, ETH Zurich, Switzerland.

04/2013 Nonequilibrium physics and phase-field modeling of multiphase flow in porous media, Department of Petroleum and Geosystems Engineering, University of Texas, Austin, TX.

04/2013 Nonequilibrium physics and phase-field modeling of multiphase flow in porous media, Department of Applied Mathematics, North Carolina State University, Raleigh, NC.

03/2013 Nonequilibrium physics and phase-field modeling of multiphase flow in porous media, Department of Civil and Environmental Engineering, Princeton University, Princeton, NJ.

02/2013 Invited talk, Nonequilibrium physics and phase-field modeling of multiphase flow in porous media, ACM Meeting, San Diego, CA.

01/2013 Invited lecture, Lifetime of carbon capture and storage as a climate change mitigation technology, Fermilab Colloquium, Fermi National Accelerator Laboratory, IL.

12/2012 Invited talk, Fingering and fracturing in granular media, American Geophysical Union (AGU) Fall Meeting, San Francisco.

05/2012 Invited talk, Fingering and fracturing in granular media, 10th Northeastern Granular Workshop, Clark University.

05/2012 Invited talk, Nonequilibrium physics of multiphase flow in porous media: fingering and fracturing in granular media, International conference on Soft Matter Physics and Complex Flows, Lofoten, Norway.

04/2012 Fingering and fracturing in granular media, DOE Geosciences Program Symposium, Gaithersburg, MD.

12/2011 Invited talk, Mixing and velocity disorder: from viscous fingering to heterogeneous media, AGU Fall Meeting, San Francisco, CA.

11/2011 Invited talk, CO2 migration and sequestration by combined capillary and solubility trapping: theory, experiments, and capacity estimates at the basin scale, Minisymposium on The Fluid Dynamics of Geological CO2 Sequestration, American Physical Society (APS) Division of Fluid Dynamics Meeting, Baltimore, MD.

10/2011 Crossover from fingering to fracturing in deformable granular media: theory and experiments, Mechanics: Modeling, Experimentation and Computation (MMEC) seminar series, Dept. of Mechanical Engineering, MIT.

10/2011 Nonequilibrium physics and computation of water infiltration in dry soil: Implications for the ecohydrology of arid regions, Computational Sustainability seminar, Computer Science and Artificial Intelligence Lab (CSAIL), MIT.

04/2011 Nonequilibrium physics of multiphase flow through porous media: Origin of gravity fingering during infiltration, Dept. of Geography and Environmental Engineering, Johns Hopkins University.

04/2011 Frontiers of Geoscience Colloquium, Nonequilibrium physics of multiphase flow through porous media: Origin of gravity fingering during infiltration, Los Alamos National Laboratory.

02/2011 Keynote lecture, Increased Deep Drainage in Arid Environments from Gravity Fingering during Infiltration, International Workshop on Interfaces and interfacial displacement processes in unsaturated porous media, Lauterbad, Germany.

10/2010 Non-equilibrium physics of multiphase flow in porous media: Origin of gravity fingers during infiltration, Dept. of Chemical Engineering, University of Florida, Gainesville, FL.

09/2010 Pattern formation during gas invasion into deformable media, Royal Netherlands Academy of Arts and Sciences (KNAW) Academy Colloquium on Multi-scale problems in sustainable resource management.

03/2010 Non-equilibrium physics of multiphase flow in porous media: Origin of gravity fingers, DOE Geosciences Program Symposium, Gaithersburg, MD.

03/2010 Keynote talk, Geological CO2 storage at the gigatonne scale, Keynote speaker and panelist, "Grand Challenges" session, Institute of Biological Engineering Annual Meeting, Cambridge, MA.

02/2010 Non-equilibrium physics of multiphase flow in porous media: Origin of gravity fingers, Earth Systems Initiative seminar series, MIT.

01/2010 Nonlocal dynamics and pattern formation in multiphase flow through porous media: Origin of gravity fingering during water infiltration, ICMS Workshop: Novel multi-scale methods for multi-phase porous media flow, Edinburgh, UK.